International Journal of Coal Geology 88 (2011) 152–162

Contents lists available at SciVerse ScienceDirect

International Journal of Coal Geology

journal homepage: www.elsevier.com/locate/ijcoalgeo

Evolution of coal permeability: Contribution of heterogeneous swelling processes

Yu Wu [a,b], Jishan Liu [b,*], Derek Elsworth [c], Hema Siriwardane [d], Xiexing Miao [a]

[a] State Key Laboratory for Geomechanics and Deep Underground Engineering, China University of Mining and Technology, Xuzhou, Jiangsu, 221008, China
[b] School of Mechanical Engineering, The University of Western Australia, WA, 6009, Australia
[c] Department of Energy and Mineral Engineering, Penn State University, USA
[d] Department of Civil & Environmental Engineering, West Virginia University, Morgantown, WV 26506-6103, USA

ARTICLE INFO

Article history:
Received 26 April 2011
Received in revised form 30 August 2011
Accepted 3 September 2011
Available online 10 September 2011

Keywords:
Coal permeability
Dual poroelasticity
Heterogeneous swelling
Fracture compaction

ABSTRACT

This study hypothesizes that coal swelling is a heterogeneous process depending on the distribution of coal voids such as fractures, and that coal matrixes swell due to CO_2 sorption while fractures are compressed in response. This explains why coal permeability reduces even when the effective stress on coal samples is kept constant. A dual porosity–dual permeability model, which separately accommodates gas flow and transport in the coal matrix (swelling component) and fracture systems (non-swelling component) and rigorously accommodates the role of mechanical deformations for a dual porosity continuum, was developed and applied to prove this hypothesis.

We use observations of a CO_2 flow-through experiment on coal constrained by X-ray CT to define the heterogeneous distribution of fracture porosity within the coal sample as a basis of mapping material properties for modeling. Matches between experimentally-measured and model-predicted ensemble permeabilities are excellent. More importantly, the model results illustrate the crucial role of heterogeneous swelling in generating swelling-induced reductions in permeability even when the fractured sample is mechanically unconstrained. These results prove that coal swelling is a heterogeneous process depending on the distribution of coal voids: matrix (swelling component) swells while fractures (non-swelling component) are compacted in response.

1. Introduction

Geological sequestration of CO_2 has been considered as one of the most promising options. Deep coal seam is one of geological media to potentially sequester huge amounts of CO_2 (Gale and Freund, 2001). The coal serves as a receptor for the injected CO_2 which is sequestered in the naturally fractured medium. The micro-pores and pores in the coal matrix provide the main storage space for gas and the micro-fractures through macro-fractures comprise rapid pathways for gas seepage and delivery to the micro-pores. In addition, sorption-induced strain of the coal matrix can change the porosity, the permeability and the storage capacity of coal seam via feedbacks to in situ stresses via displacement constraints. Correspondingly, the evolution of in situ stress conditions have an important influence on reservoir response and capacity for CO_2 storage, inferring that both flow and mechanical interactions should be incorporated if realistic simulations of behavior are desired. This study addresses this complex and challenging problem.

The dominance of fluid flow in fractures is exhibited in fractured crystalline rocks, such as granite, where matrix blocks contribute negligible fluid mass to the highly conductive fractures. However, gas flow in unconsolidated materials such as coal is essentially interstitial where flow routes may be rather tortuous. The fractured coal seam comprises both permeable fractures and matrix blocks. Gas flow in such a medium may be intermediate between fracture flow and interstitial flow. Dual porosity representations (Barrenblatt et al., 1960; Warren and Root, 1963) include the response of these two principal components only — release from storage in the porous matrix and transport in the fracture network. Conversely, dual permeability or multiple permeability models represent the porosity and permeability of all constituent components (Bai et al., 1993) including the role of sorption (Bai et al., 1997) and of multiple fluids (Douglas et al., 1991). Traditional flow models accommodate the transport response as overlapping continua but neglect mechanical effects. In situations where mechanical effects are important, this behavior must be included in the response. Conceptualizations include analytical models for dual porosity media with averaged elastic components (Aifantis, 1977), their numerical implementation and models including the component constitutive response for dual (Elsworth and Bai, 1992) and multi-porous (Bai et al., 1993) media. Such models have been applied to represent the response of permeability evolution (Liu and Elsworth, 1999; Ouyang and Elsworth, 1993) in deforming aquifers and reservoirs (Bai et al., 1995), to accommodate gas flow (Zhao et al.,

* Corresponding author. Tel.: +61 8 6488 7205.
E-mail address: Jishan@cyllene.uwa.edu.au (J. Liu).

0166-5162/$ – see front matter © 2011 Elsevier B.V. All rights reserved.
doi:10.1016/j.coal.2011.09.002

2004) and to evaluate the response to external forcing by human-induced effects (Liu and Elsworth, 1999) and by earth tides (Pili et al., 2004).

All of these previous models were developed primarily for the flow of slightly compressible liquids without desorption and not applicable to the flow of compressible fluids such as CO_2 where gas adsorption is the dominant mechanism. The potential impacts of differential swelling on the performance and implementation of CO_2 geological sequestration projects have been investigated through experimental, field-scale, and numerical studies. Experiments on powdered high volatile bituminous Pennsylvanian coals have shown that adsorption rate decreases with increasing grain size for all experimental conditions (Busch et al., 2004). Similarly, coal type and rank (Prusty, 2007; Robertson and Christiansen, 2005) influences the preferential sorption behavior and the evolution of permeability with these changes linked to macromolecular structure (Mazumder and Wolf, 2007). The impacts of gas components on the efficiency of enhanced methane recovery have also been investigated, indicating that the presence of the nitrogen originating from flue gas in the injected gas stream is capable of improving the injectivity significantly (Durucan and Shi, 2008). The adsorption kinetics of CO_2 and CH_4 at different pressures and temperatures have been explored (Charrièrea et al., 2010). Similarly, the sorption and swelling capacities of CO_2 under supercritical conditions have been examined on a variety of dry and wet coals with different pressures and temperatures (Day et al., 2008; Siemons and Busch, 2007). Distributed measurements of the sorption of CO_2 have shown temporal influences of diffusion into dual porosity media (Karacan, 2007) and the role of ambient stress in modulating swelling-induced strain (Pone et al., 2008).

Based on experimental observations, a variety of models have been formulated to quantify the evolution of permeability during coal swelling/shrinkage. The first attempts to quantify the role of stresses on the evolution of coal-reservoir permeability assumed invariant vertical stresses and linked changes in horizontal stress with the gas pressure and the sorption strain (Gray, 1987). Permeability was computed as a function of reservoir pressure with coal-matrix shrinkage assumed directly proportional to changes in the equivalent sorption pressure. Since then, a number of theoretical and empirical permeability models have been proposed. The Seidle–Huitt Model describes the evolution of permeability assuming that all changes in permeability are caused by the sorption-induced strain alone, neglecting the elastic strain (Seidle and Huitt, 1995). Another three of the most widely used permeability models are the Palmer and Mansoori model (P&M Model), the Shi and Durucan (S&D) model, and the Advanced Resources International (ARI) model (Palmer and Mansoori, 1998; Pekot and Reeves, 2003; Shi and Durucan, 2005). The P&M model is strain-based, which means that porosity change is modulated by the change in the volume strain, and the change in permeability is calculated from this change in porosity. It is derived from linear elasticity for strain changes in porous rock assuming no change in overburden stress, that changes in porosity are small and also that the permeating fluid is highly compressible. A cubic relationship between permeability and porosity is used to evaluate changes in permeability. The S&D model is based on an idealized bundled-matchstick geometry to represent a coalbed, and uses a stress-based formulation to correlate changes in the effective horizontal stress caused by the volumetric deformation together with the cleat or pore compressibilities. This stress-based model means that changes in porosity and permeability do not come directly from changes in volume strain but via the swelling-induced augmentation of horizontal stresses. Additionally, the Biot coefficient is set to unity — requiring that the change in net stress is equal to the difference between net overburden pressure and the change in pore pressure. The ARI model describes the evolution of coal permeability using a semi-empirical correlation to account for the changes of coal porosity due to pore compressibility and matrix swelling/shrinkage (Pekot and Reeves, 2003). The ARI model is essentially equivalent to the P&M model in saturated coal and where the strain versus stress fits the Langmuir isotherm (Palmer, 2009). More recently, an alternative approach has been proposed to develop an improved permeability model for CO_2-ECBM recovery and CO_2 geo-sequestration in coal seams. This approach integrates textural and mechanical properties to describe the anisotropy of gas permeability in coal reservoirs under conditions of confined stress (Wang et al., 2009). However, although permeability models incorporating sorption-induced effects have been widely studied, those studies are under the assumption of either a constant overburden load, or derived from the compressibility concept of porosity, which may provide incorrect outcomes or overestimates of permeability change (Pekot and Reeves, 2003; Robertson and Christiansen, 2007). These critical and limiting assumptions have been relaxed in new models rigorously incorporating in-situ stress conditions (Zhang et al., 2008). More importantly, coal is highly anisotropic: both in mechanical properties and permeability. The micro-fractures and cleats in coal are quite different in each direction. Directional permeability cannot be described using a scalar porosity variable, especially for the fracture permeability (Wang et al., 2009).

CO_2 injection into coal seams triggers complex coal–gas interactions because of the phenomena of gas adsorption and coal swelling. The relative roles of stress level, gas pressure, and fracture distribution are intimately connected to the processes of gas adsorption, diffusion, transport, and coal swelling. Although this phenomenon has been studied widely, majority of prior studies are under the assumptions of no change in overburden stress or effective stress-absent and the heterogeneous effects are rarely considered.

As observed in previous studies (Karacan, 2003, 2007; Karacan and Mitchell, 2003), the CO_2 sorption-associated swelling and volumetric strains in consolidated coal under constant effective stress are heterogeneous processes depending on the lithotypes present. In the time scale of the experiment, vitrite showed the highest degree of swelling due to dissolution of CO_2, while the clay (kaolinite) and inertite region was compressed in response. The volumetric strains associated with swelling and compression were between $\pm 15\%$ depending on the location. These observations may have implied that the swelling component of matrix swells while the non-swelling component of matrix is compacted in response. This provides the basis to assume that coal swelling is a heterogeneous process depending on the distribution of coal voids such as fractures, and that coal matrixes show the highest degree of swelling due to dissolution of CO_2 while fractures are compressed in response. In this study, we extended our previous work (Liu et al., 2010a,b; Wu et al., 2009; Wu et al., 2010a,b) to represent heterogeneous swelling processes through the inclusion of spatially-distributed fracture porosity into complex interactive phenomena (mechanical coupling with gas transport).

2. Governing equations

The set of field equations for coupled coal deformation and gas flow are defined in the following. These field equations are coupled through new porosity and permeability models to represent the response of coal matrix and fractures. These derivations are based on the assumptions that:

(a) Coal is a dual poroelastic continuum.
(b) Strains are much smaller than the length scale.
(c) Gas contained within the pores is ideal, and its viscosity is constant under isothermal conditions.
(d) Conditions are isothermal.
(e) Compositions of the gas are not competitive, i.e., one gas component is considered at time.

In the following derivations, the fractured coal is conceptualized as in Fig. 1. It comprises coal matrix and fractures. The edge dimension of the matrix blocks and the fracture aperture are represented

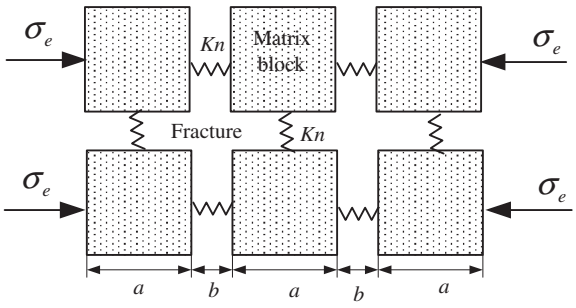

Fig. 1. Dual-porosity fractured medium.

by a and b, respectively. K_n is the fracture stiffness, and σ_e is the effective stress.

2.1. Coal deformation

Based on our previous work (Wu et al., 2010a,b), the governing equation for coal deformation can be defined as

$$Gu_{i,kk}+\frac{G}{1-2\nu}u_{k,ki}-\alpha p_{m,i}-\beta p_{f,i}-K\varepsilon_{s,i}+f_i=0 \quad (1)$$

where, G is shear stiffness, p is gas pressure, the subscript m represents the matrix and f the fracture system, ε_s is gas sorption-induced strain, α, β are the Biot coefficients (Biot, 1941), K is the bulk modulus and δ_{ij} is the Kronecker delta.

For a system containing a single gas phase the sorption-induced volumetric strain ε_s may be represented by a Langmuir type function (Cui and Bustin, 2005; Harpalani and Schraufnagel, 1990; Robertson and Christiansen, 2007), defined as

$$\varepsilon_s=\varepsilon_L\frac{p_m}{P_L+p_m} \quad (2)$$

where ε_L and P_L are the Langmuir-type matrix swelling/shrinkage constants, which represent the maximum swelling capacity and the pore pressure at which the measured volumetric strain is equal to $0.5\varepsilon_L$, respectively. Both parameters are related to reservoir temperature.

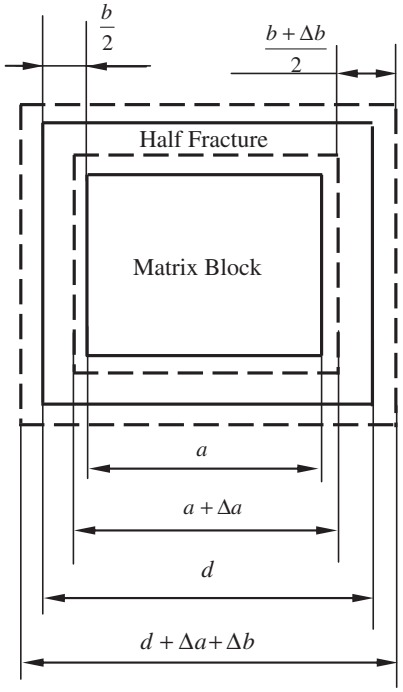

Fig. 2. Schematic of coal matrix within the REV.

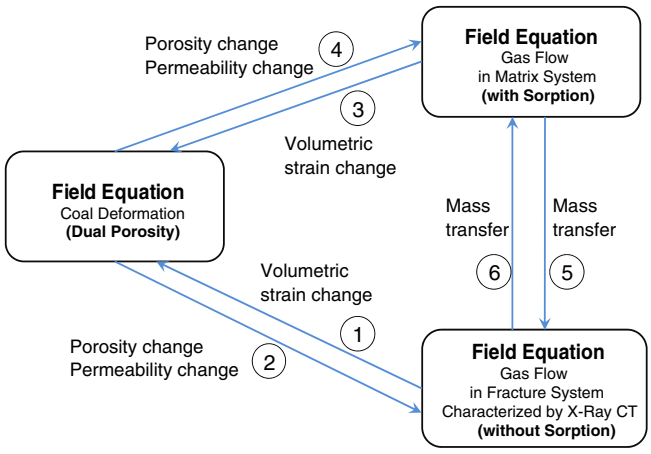

Fig. 3. Cross coupling of the field equations.

2.2. Gas flow

Based on our previous work (Wu et al., 2010a,b), the governing equations for gas flow in coal matrix and fracture can be defined as

$$\left[\phi_m+p_{ga}\rho_c\frac{V_L p_m}{p_m+p_L}\right]\frac{\partial p_m}{\partial t}+p_m\frac{\partial\phi_m}{\partial t}+\nabla\cdot\left(-\frac{k_m}{\mu}p_m\nabla\cdot p_m\right)=\omega\left(p_f-p_m\right) \quad (3)$$

$$\phi_f\frac{\partial p_f}{\partial t}+p_f\frac{\partial\phi_f}{\partial t}+\nabla\cdot\left(-\frac{k_f}{\mu}p_f\nabla\cdot p_f\right)=-\omega\left(p_f-p_m\right) \quad (3)$$

where, P_a is the standard atmosphere pressure and ω is the transfer coefficient defined as

$$\omega=8\left(1+\frac{2}{a^2}\right)\frac{k_m}{\mu}. \quad (4)$$

In Eqs. (3) and (4), the porosities for matrix and fracture, ϕ_m and ϕ_f, and the permeability for the matrix and the fracture, k_m and k_f change with the effective stress, σ_e, and the sorption-induced strain, ε_s. In the representation of coal deformation (Eq. 1), p_m (gas pressure in the matrix), p_f (gas pressure in the fracture), and ε_s (gas sorption

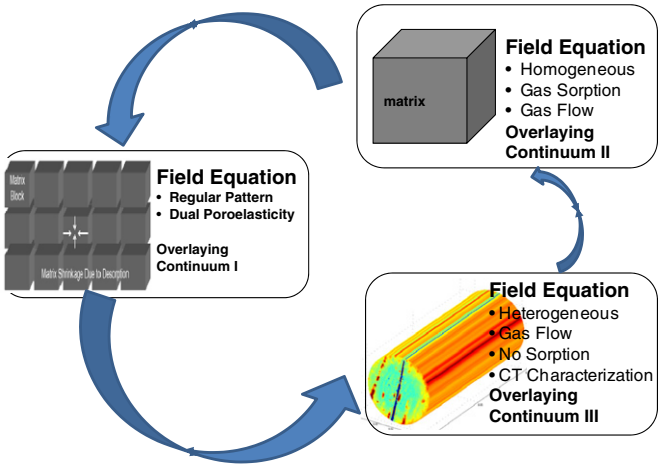

Fig. 4. Characterizations of three overlaying continua for coal matrix system, coal fracture system, and coal deformation.

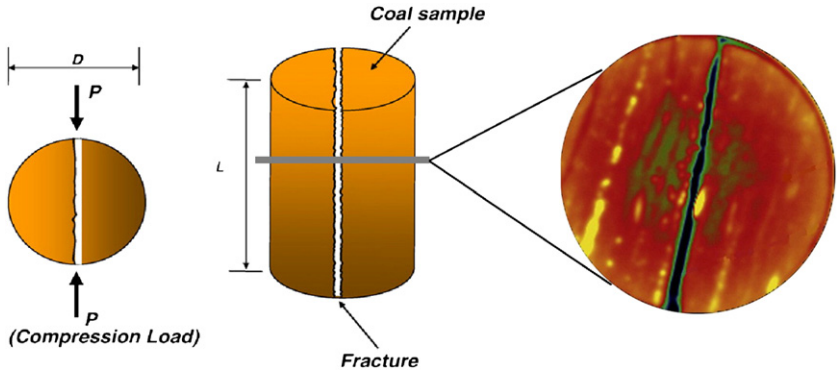

Fig. 5. The induced fracture through a coal sample and a typical CT scan (Siriwardane et al., 2009).

strain), are linked to the gas flow equations. Therefore, Eqs. (1) and (3)–(4) define the coupled gas flow and coal deformation model for a dual-porosity medium.

2.3. Dynamic permeability model for coal matrix

The porosity and permeability of the fracture are controlled primarily by the aperture of the cleats. In order to analyze the change of fracture aperture, we consider a representative elemental volume (REV) from the dual-porosity model as an example. As shown in Fig. 2, the matrix block fills the center of the repeating REV with a half fracture surrounding the matrix block on all sides. The solid lines are the outline of the REV pre-deformation and the dashed lines are the outline of the REV post-deformation.

As shown in Fig. 2, the deformations of the matrix and fracture are defined as follows

$$\begin{aligned} \Delta d &= \Delta b + \frac{a\varepsilon_m}{3} \\ \varepsilon &= \frac{b}{a}\frac{\varepsilon_f}{3} + \frac{\varepsilon_m}{3} \end{aligned} \tag{5}$$

where, ε is the total uni-directional strain of the REV, ε_f and ε_m are the strains of fracture and matrix, respectively. b is the aperture of the fracture, a is the length of the REV and d is the sum of a and b. Because $a>>b$ then $d=a+b\approx a$.

There are three kinds of effects that affect the coal deformation during the CO_2 injection: (i) Thermal effects $f(\Delta T)$; (ii) Chemical/sorption effects $f(\Delta c, \Delta p)$; and (iii) Effective stress effects $f(\Delta\sigma_e)$. Therefore, the free-strain of the matrix can be defined as the sum of these serial processes as

$$\varepsilon_m = \alpha_T \Delta T + \varepsilon_L\left(\frac{p_m}{p_L+p_m} - \frac{p_{m0}}{p_L+p_{m0}}\right) - \frac{1}{K}\Delta\sigma_m \tag{6}$$

where α_T is the thermal expansion coefficient. ε_L is the Langmuir constant representing the volumetric strain at infinite pressure. $\Delta\sigma_m$ is the stress the fracture exerts on the matrix and p_{m0} is the initial pressure in the matrix. Ignoring the effects of sorption and thermal expansion within the fracture, the strain within the fracture can be defined as

$$\varepsilon_f = -\frac{1}{K}\Delta\sigma_f \tag{7}$$

where $\Delta\sigma_f$ is the stress applied by the matrix onto the fracture. The total strain within the REV yields

$$\varepsilon = \frac{1}{3}\left[\alpha_T\Delta T + \varepsilon_L\left(\frac{P_m}{P_L+P_m} - \frac{P_{m0}}{P_L+P_{m0}}\right) - \frac{b_0}{aK_f}\Delta\sigma_f - \frac{1}{K}\Delta\sigma_m\right] \tag{8}$$

where, K_f is the modified fracture stiffness, $K_f = aK_n$. Subscript f represents that the parameter relates to the fracture.

Assuming the volumetric strain of the REV is ε_v, we obtain

$$\varepsilon_v = 3\varepsilon \tag{9}$$

Therefore, Eq. (8) can be rewritten as

$$\alpha_T\Delta T + \varepsilon_L\left(\frac{P_m}{P_L+P_m} - \frac{P_{m0}}{P_L+P_{m0}}\right) - \frac{b_0}{aK_f}\Delta\sigma_f - \frac{1}{K}\Delta\sigma_m = \varepsilon_v. \tag{10}$$

To satisfy force equilibrium the total stresses in the fracture and matrix are the same, i.e., $\Delta\sigma_f = \Delta\sigma_m = \Delta\sigma_e$. Eq. (10) may be simplified as

$$\alpha_T\Delta T + \varepsilon_L\left(\frac{P_m}{P_L+P_m} - \frac{P_{m0}}{P_L+P_{m0}}\right) - \left(\frac{b_0}{aK_f} + \frac{1}{K}\right)\Delta\sigma_e = \varepsilon_v. \tag{11}$$

Then, the change in effective stress is defined as

$$\Delta\sigma_e = \frac{1}{N}\left(\alpha_T\Delta T + \frac{\varepsilon_L P_L(P_m - P_{m0})}{(P_L+P_m)(P_L+P_{m0})} - \varepsilon_v\right) \tag{12}$$

where, $N = \frac{b_0}{aK_f} + \frac{1}{K}$.

It is apparent from Eq. (12) that the change in effective stress results from the effect of sorption. Considering a porous medium containing solid volume of V_s and pore volume V_p, we assume the bulk volume $V = V_s + V_p$ and the matrix porosity $\varphi_m = V_p/V$. Substituting Eq. (12) into Eq. (6) and ignoring the thermal effect, yields

$$\varepsilon_m = -\frac{\Delta V}{V} = \frac{\varepsilon_L P_L(P_m - P_{m0})}{(P_L+P_m)(P_L+P_{m0})} - \frac{1}{K}\cdot\frac{1}{N}\left(\frac{\varepsilon_L P_L(P_m - P_{m0})}{(P_L+P_m)(P_L+P_{m0})} - \varepsilon_v\right). \tag{13}$$

The sorption-induced volumetric strain for the pore volume is assumed to be the same as for the bulk medium (Zimmerman et al., 1986). The strain of pore can be expressed as

$$\varepsilon_p = -\frac{\Delta V_p}{V_p} = \frac{\varepsilon_L P_L(P_m - P_{m0})}{(P_L+P_m)(P_L+P_{m0})} - \frac{1}{K_p}\cdot\frac{1}{N}\left(\frac{\varepsilon_L P_L(P_m - P_{m0})}{(P_L+P_m)(P_L+P_{m0})} - \varepsilon_v\right) \tag{14}$$

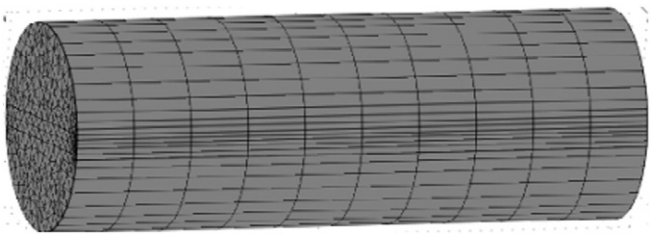

Fig. 6. Mesh representing the sample.

Table 1
Material properties of the coal sample.

Sample no.	D_{sample} (mm)	L_{sample} (mm)	Porosity	Pore pressure (MPa)	Confining pressure (MPa)
S08	37.46	77.1	0.27%	10.0	20.0

where K_p is the modulus of the pores. Without the gas sorption effect, the volumetric variation of the porous medium satisfies the Betti–Maxwell reciprocal theorem (Detournay and Cheng, 1993), and then we obtain

$$K_p = \frac{\phi_m K}{\alpha}. \tag{15}$$

Using the definition of porosity, the porosity change of a deforming coal seam can be described as

$$d\phi_m = d\left(\frac{V_p}{V}\right) = \frac{V_p}{V}\left(\frac{dV_p}{V_p} - \frac{dV}{V}\right). \tag{16}$$

Substituting Eqs. (13)–(14) into Eq. (16) yields

$$d\phi_m = \frac{\phi_m - \alpha}{K}\left(d\varepsilon_m - d\varepsilon_p\right). \tag{17}$$

As coal is a typical porous medium, the bulk modulus of coal matrix K is much smaller than the modulus of coal grains. Therefore, based on the definition of the Biot coefficient, we obtain $\varphi_m << \alpha$. Simplifying Eq. (17) and integrating with time yields

$$\phi_m = \phi_{m0} - \frac{\alpha}{K}\cdot\frac{1}{\frac{b_0}{aK_f}+\frac{1}{K}}\left(\frac{\varepsilon_L P_L (P_m - P_{m0})}{(P_L+P_m)(P_L+P_{m0})} - \varepsilon_v\right). \tag{18}$$

It is clear that there is a relationship between porosity, permeability and grain-size distribution of porous medium. Chilingar, (1963) defined this relationship as

$$k_m = \frac{d_e^2 {\phi_m}^3}{72(1-\phi_m)^2} \tag{19}$$

where, k_m is the matrix permeability, φ_m is matrix porosity and d_e is the effective diameter of the grains. Based on this equation, we can obtain

$$\frac{k_m}{k_{m0}} = \left(\frac{\phi_m}{\phi_{m0}}\right)^3 \left(\frac{1-\phi_{m0}}{1-\phi_m}\right)^2 \tag{20}$$

when the porosity is much smaller than 1 (normally less than 10%), the second term on the right side can be ignored. Then we have the cubic relationship of permeability and porosity can be also use for matrix.

$$\frac{k_m}{k_{m0}} = \left(\frac{\phi_m}{\phi_{m0}}\right)^3 \tag{21}$$

Substituting Eq. (18) into Eq. (21), the permeability model for the matrix can be obtained as

$$\frac{k_m}{k_{m0}} = \left(1 - \frac{\alpha}{\phi_{m0}K}\cdot\frac{1}{\frac{b_0}{aK_f}+\frac{1}{K}}\left(\frac{\varepsilon_L P_L (P_m - P_{m0})}{(P_L+P_m)(P_L+P_{m0})} - \varepsilon_v\right)\right)^3. \tag{22}$$

2.4. Dynamic permeability model for fracture

For the fracture system, the fracture porosity and permeability can be calculated from the fracture spacing and aperture as (Liu et al., 1999)

$$\phi_f = \frac{(a+b)^3 - a^3}{(a+b)^3} \cong \frac{3b}{a} \tag{23}$$

$$\frac{\phi_f}{\phi_{f0}} = 1 + \frac{\Delta b}{b_0}. \tag{24}$$

Apparent from Eq. (12) the change in effective stress results from the influence of sorption. Since the change in effective stress has already been determined, fracture opening may be obtained as

$$\Delta b = -\frac{b_0}{K_f}\Delta\sigma_e = -\frac{b_0}{K_f}\frac{1}{A}\left(\alpha_T \Delta T + \frac{\varepsilon_L \Delta P_m}{P_L + \Delta P_m} - \varepsilon_v\right) \tag{25}$$

Substituting Eq. (25) into Eq. (24), yields the dynamic porosity model for the fracture as

$$\frac{\phi_f}{\phi_{f0}} = 1 + \frac{\Delta b}{b_0} = 1 - \frac{3}{\phi_{f0} + \frac{3K_f}{K}}\left(\frac{\varepsilon_L P_L (P_m - P_{m0})}{(P_L+P_m)(P_L+P_{m0})} - \varepsilon_v\right). \tag{26}$$

Based on the cubic relation between fracture porosity and permeability, the dynamic permeability model for fracture can be defined as

$$\frac{k_f}{k_{f0}} = \left(\frac{\phi_f}{\phi_{f0}}\right)^3 = \left(1 - \frac{3}{\phi_{f0} + \frac{3K_f}{K}}\left(\frac{\varepsilon_L P_L (P_m - P_{m0})}{(P_L+P_m)(P_L+P_{m0})} - \varepsilon_v\right)\right)^3. \tag{27}$$

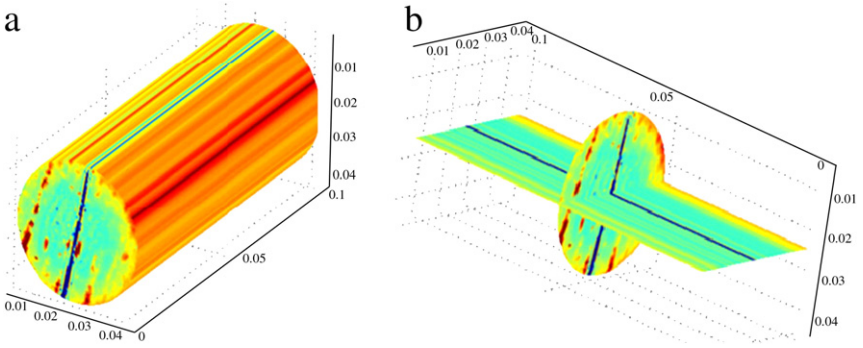

Fig. 7. Virtual core: (a) 3D view; (b) cross-sectional views.

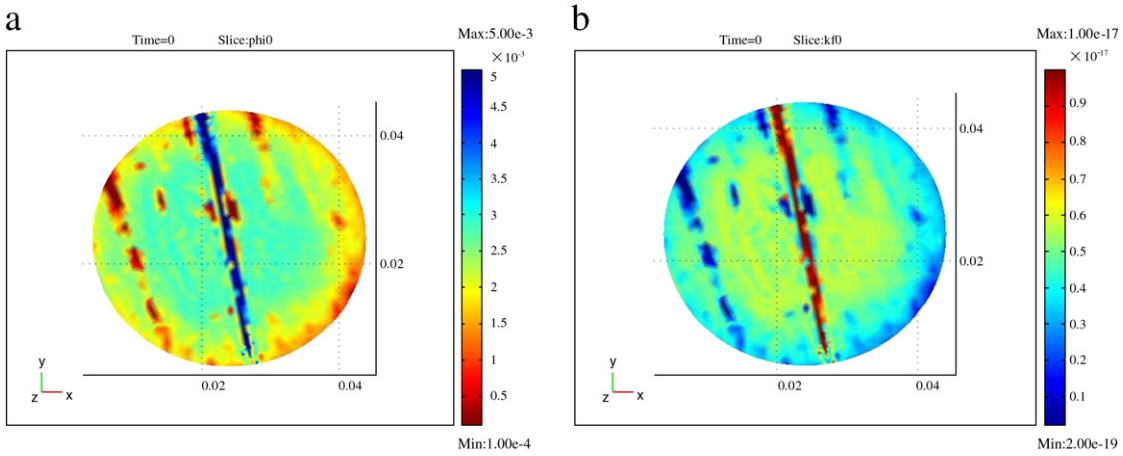

Fig. 8. Initial properties of coal sample: (a) initial porosity distribution; (b) initial permeability distribution.

Similarly, from the previous, we can derive the directional permeability of fracture as

$$\begin{cases} \dfrac{k_{fx}}{k_{f0}} = \dfrac{1}{2}\left(1-\dfrac{1}{\phi_{f0}+\dfrac{3K_f}{K}}\left(\dfrac{\varepsilon_L P_L(P_m-P_{m0})}{(P_L+P_m)(P_L+P_{m0})}-3\varepsilon_y\right)\right)^3 \\ \qquad +\dfrac{1}{2}\left(1-\dfrac{1}{\phi_{f0}+\dfrac{3K_f}{K}}\left(\dfrac{\varepsilon_L P_L(P_m-P_{m0})}{(P_L+P_m)(P_L+P_{m0})}-3\varepsilon_z\right)\right)^3 \\ \dfrac{k_{fy}}{k_{f0}} = \dfrac{1}{2}\left(1-\dfrac{1}{\phi_{f0}+\dfrac{3K_f}{K}}\left(\dfrac{\varepsilon_L P_L(P_m-P_{m0})}{(P_L+P_m)(P_L+P_{m0})}-3\varepsilon_x\right)\right)^3 \\ \qquad +\dfrac{1}{2}\left(1-\dfrac{1}{\phi_{f0}+\dfrac{3K_f}{K}}\left(\dfrac{\varepsilon_L P_L(P_m-P_{m0})}{(P_L+P_m)(P_L+P_{m0})}-3\varepsilon_z\right)\right)^3 \\ \dfrac{k_{fz}}{k_{f0}} = \dfrac{1}{2}\left(1-\dfrac{1}{\phi_{f0}+\dfrac{3K_f}{K}}\left(\dfrac{\varepsilon_L P_L(P_m-P_{m0})}{(P_L+P_m)(P_L+P_{m0})}-3\varepsilon_x\right)\right)^3 \\ \qquad +\dfrac{1}{2}\left(1-\dfrac{1}{\phi_{f0}+\dfrac{3K_f}{K}}\left(\dfrac{\varepsilon_L P_L(P_m-P_{m0})}{(P_L+P_m)(P_L+P_{m0})}-3\varepsilon_y\right)\right)^3 . \end{cases} \tag{28}$$

Table 2
Material parameters used in the simulation model.

Parameter	Value
Young's modulus of coal (E, GPa)	2.71
Young's modulus of coal grains (E_s, GPa)	8.13
Possion's ratio of coal (ν)	0.34
Density of coal (ρ_c, kg/m^3)	1.25×10^3
Gas dynamic viscosity (μ, Pa·s)	1.84×10^{-5}
CO_2 Langmuir volume constant (V_L, m^3/kg)	0.0477
CO_2 Langmuir volumetric strain constant (ε_L)	0.0237
CO_2 Langmuir pressure constant (p_L, MPa)	1.38
Initial porosity of matrix (ϕ_{m0})	0.0027
Initial porosity of fracture (ϕ_{f0})	From CT image
Initial permeability of matrix (k_{m0}, m^2)	3.0×10^{-19}
Initial permeability of fracture (k_{f0}, m^2)	From CT image

2.5. Cross coupling

For convenience, the governing equation for coal deformation is re-written as follows:

$$Gu_{i,kk}+\frac{G}{1-2\nu}u_{k,ki}-\alpha p_{m,i}-\beta p_{f,i}-K\varepsilon_L\frac{p_L}{(p_m+p_L)^2}p_{m,i}+f_i=0. \tag{29}$$

Substituting the partial derivatives of ϕ_m and ϕ_f with respect to time from Eqs. (18), (26) and the permeability Eqs. (22) and (27) into the gas flow Eqs. (3) and (4), yields the final gas flow equations:

$$\left[\phi_m+(1-\phi_{m0})p_{ga}\rho_c\frac{V_L p_L}{(p_m+p_L)^2}-\frac{\alpha K_f}{\dfrac{b_0}{a}K+K_f}\cdot\frac{\varepsilon_L p_L p_m}{(p_m+p_L)^2}\right]\frac{\partial p_m}{\partial t} +\frac{\alpha K_f}{\dfrac{b_0}{a}K+K_f}p_m\frac{\partial\varepsilon_v}{\partial t}+\nabla\cdot\left(-\frac{k_m}{\mu}p_m\nabla p_m\right)=\omega\left(p_f-p_m\right) \tag{30}$$

$$\phi_{f0}\left[1-\frac{3}{\phi_{f0}+\dfrac{3K_f}{K}}\left(\frac{\varepsilon_L P_L(P_m-P_{m0})}{(P_L+P_m)(P_L+P_{m0})}-\varepsilon_v\right)\right]\frac{\partial p_f}{\partial t}-\frac{3\phi_{f0}p_f}{\phi_{f0}+\dfrac{3K_f}{K}}\cdot\frac{\varepsilon_L P_L}{(P_L+P_m)^2}\frac{\partial p_m}{\partial t} +\frac{3\phi_{f0}p_f}{\phi_{f0}+\dfrac{3K_f}{K}}\frac{\partial\varepsilon_v}{\partial t}+\nabla\cdot\left(-\frac{k_f}{\mu}p_f\nabla p_f\right)=-\omega\left(p_f-p_m\right). \tag{31}$$

Eqs. (29), (30) and (31) define the coal deformation, gas transport in the coal matrix, and gas flow in the coal fracture, respectively. These three equations are coupled through two permeability models as defined by Eqs. (22) and (27). Detailed interactions between gas transport in the matrix system, coal deformation in the dual poroelastic continuum, and gas flow in the fracture system are illustrated in Fig. 3 and summarized as follows:

(1) The interaction between coal deformation and gas flow in the fracture is defined by term $-\beta p_{f,i}$. This term represents the change of effective stress induced by pressure change in the fracture system, and affects the volumetric strain of coal.
(2) The interaction between coal deformation and gas flow in the fracture is also defined by other two terms, $\frac{3K\phi_{f0}p_f}{\phi_{f0}K+3K_f}\frac{\partial\varepsilon_v}{\partial t}$ and $\frac{k_f}{k_{f0}}$. These two terms represent the porosity change and the permeability change induced by the coal deformation.

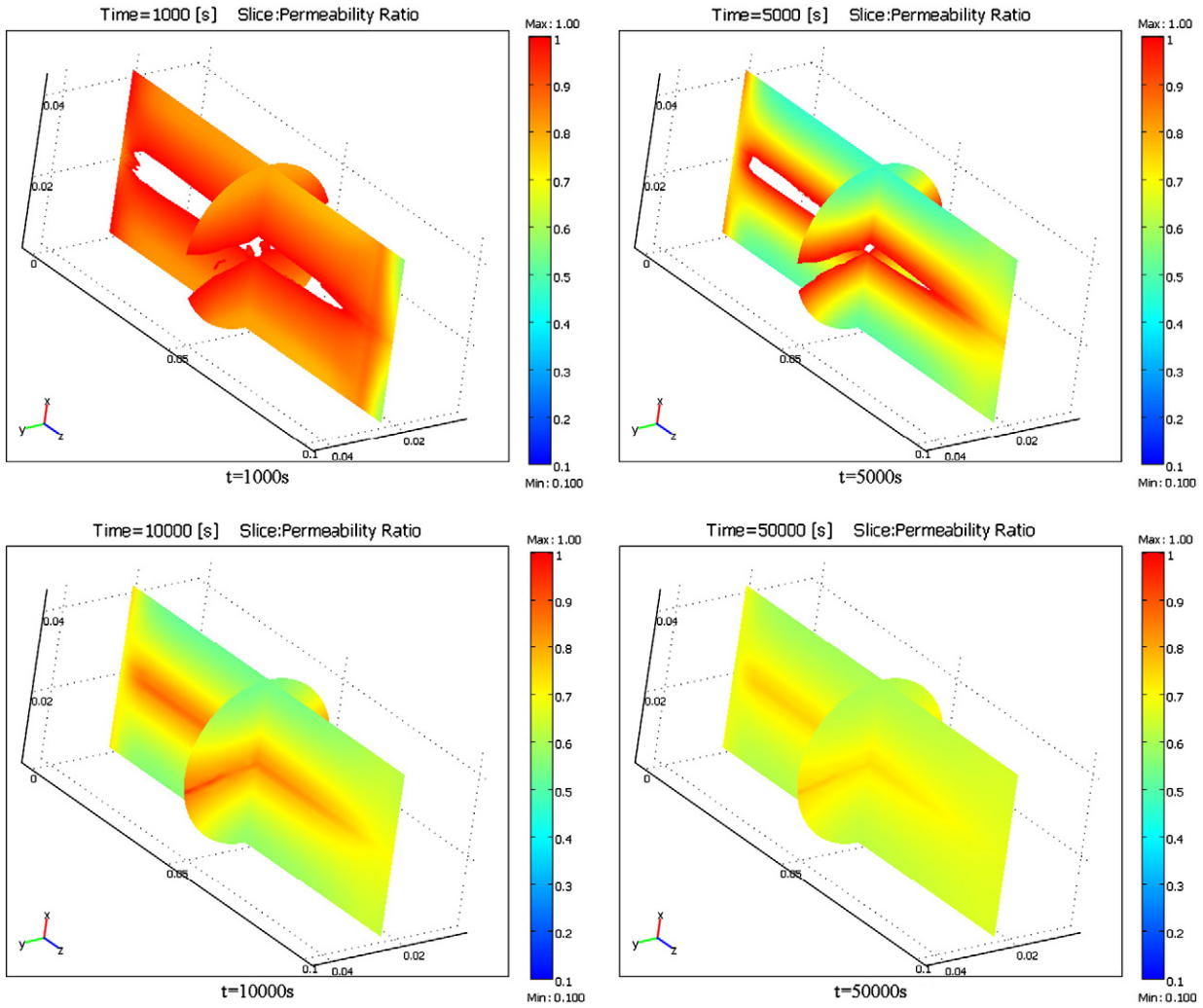

Fig. 9. Characteristics of the permeability ratio.

(3) The interaction between coal deformation and gas flow in the matrix is defined by term $-\alpha p_{m,i} - K\varepsilon_L \frac{p_L}{(p_m+p_L)^2} p_{m,i}$. This term represents the change of effective stress induced by pressure change and coal swelling in the matrix, and affects the change in volumetric strain of coal.

(4) The interaction between coal deformation and gas flow in the matrix is also defined by other two terms, $\frac{\alpha a K_f p_m}{b_0 K + a K_f} \frac{\partial \varepsilon_v}{\partial t}$ and $\frac{k_m}{k_{m0}}$. These two terms represent the porosity change and the permeability change in the matrix due to the coal deformation.

(5) The interaction between gas flow in the fracture and gas flow in the matrix is defined by term $\omega(p_f - p_m)$. This term represents the gas mass transfer between the two systems.

(6) The interaction between gas flow in the fracture and gas flow in the matrix is also defined by term $-\omega(p_f - p_m)$. This term represents the gas mass transfer between the two systems.

3. Modeling approach

As discussed previously, the distribution of fractures has a crucial impact on the evolution of swelling processes. This behavior may be adequately represented by a dual porosity–dual permeability model. This formulation involves three overlaying continua: coal, gas flow in matrix, and gas flow in fracture. Their characterizations are illustrated in Fig. 4. For coal deformation, a cubic coal model is assumed with matrix blocks completely separated from each other in a coal sample. For gas flow and transport in the matrix system, a homogeneous coal model is used. For gas flow and transport in the fracture system, a "virtual" fracture distribution model, as characterized by CT-scans, is reconstructed.

Siriwardane et al. (2009) carried out a series of experiments to investigate the permeability of coal sample by injecting carbon dioxide. Samples were obtained from Pittsburgh seam near the research laboratory. In order to investigate the influence of CO_2 exposure on coal permeability, each coal core sample was induced a fracture to increase the

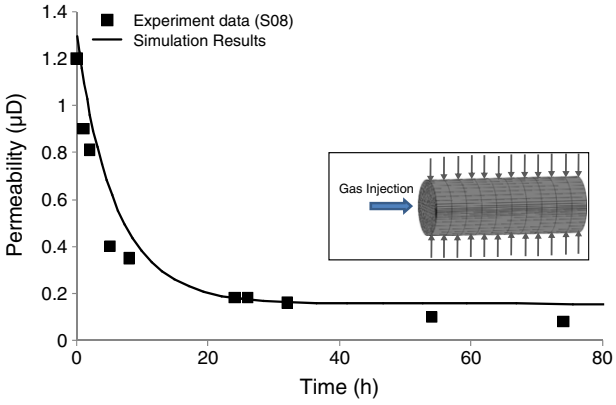

Fig. 10. Permeability evolution of the coal sample.

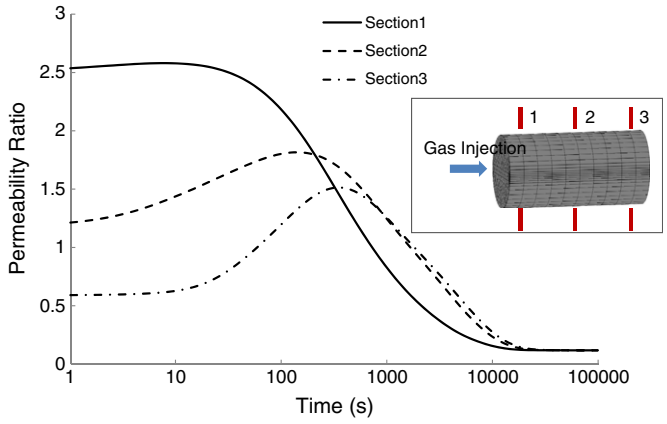

Fig. 11. Permeability ratios at different cross sections of the coal sample.

initial permeability by applying a compression load on the cylindrical surface. X-ray CT images were taken to show the induced fracture distribution inside the coal sample as illustrated in Fig. 5.

In order to compare the simulation results with the experimental data, we use the images for the coal sample to re-construct the core for numerical testings (Fig. 6). The basic parameters of the sample are shown in Table 1. The virtual core representing the sample is cylindrical with a radius of 20 mm and a length of 100 mm. The voxel distribution from the CT image is used to define the initial fracture distribution for the finite element model. The characteristics of the initial fracture are shown in Fig. 7. The initial porosity and permeability of fracture system are calculated from the color value of CT image with a threshold method (Chang et al., 2008), as shown in Fig. 8. Because this is a coupled coal deformation and gas flow problem, boundary and initial conditions are required for each component model. For the coal deformation model, the bottom face is fixed while the top face is free. A constant confining pressure of 10 MPa was applied around the cylinder. For the gas flow, a constant injection pressure of 10 MPa is applied to the top face. No flow conditions are applied to all the other boundary faces. Input properties are listed in Table 2. Some of the properties were from the coal sample experiment (Siriwardane et al., 2009). The others were chosen from the literature (Robertson and Christiansen, 2005).

4. Simulation results

We first match the model ensemble permeability with the experimentally-measured ones. This verifies the validity of the virtual core model. The verified model is then applied to investigate the dynamic processes that contribute to observed changes in permeability.

4.1. Characteristics of mechanical response

Fig. 9 shows the permeability ratio distribution for the whole domain. In order to compare the results at different times we set the color bars with the same distribution (0.1–1). The null region in the first two figures identifies regions where the permeability ratio (k/k_0) is larger than 1. When t = 1000 s the null region is large and significantly envelops the fracture. This effect is largest at the injection end where effective stresses are reduced the greatest — to zero effective stress at the injection point. With time, this volume of permeability increase diminishes until at t = 10,000 s the null area disappears altogether — in this instance the permeability everywhere within the domain has decreased from the initial condition. However, even in this condition, the permeability close to the fracture remains the largest. At about 50,000 s, this region becomes very small and the permeability in the whole sample becomes relatively uniform. The

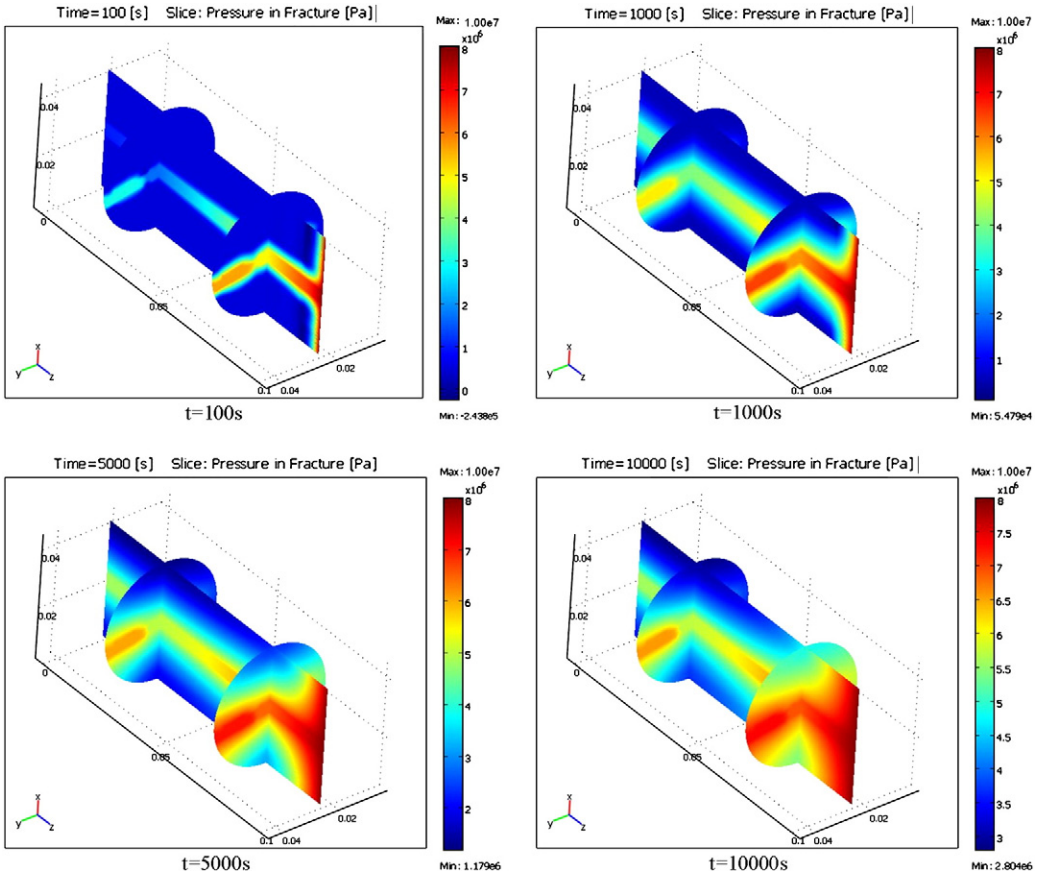

Fig. 12. Characteristics of pressure distribution in the fracture.

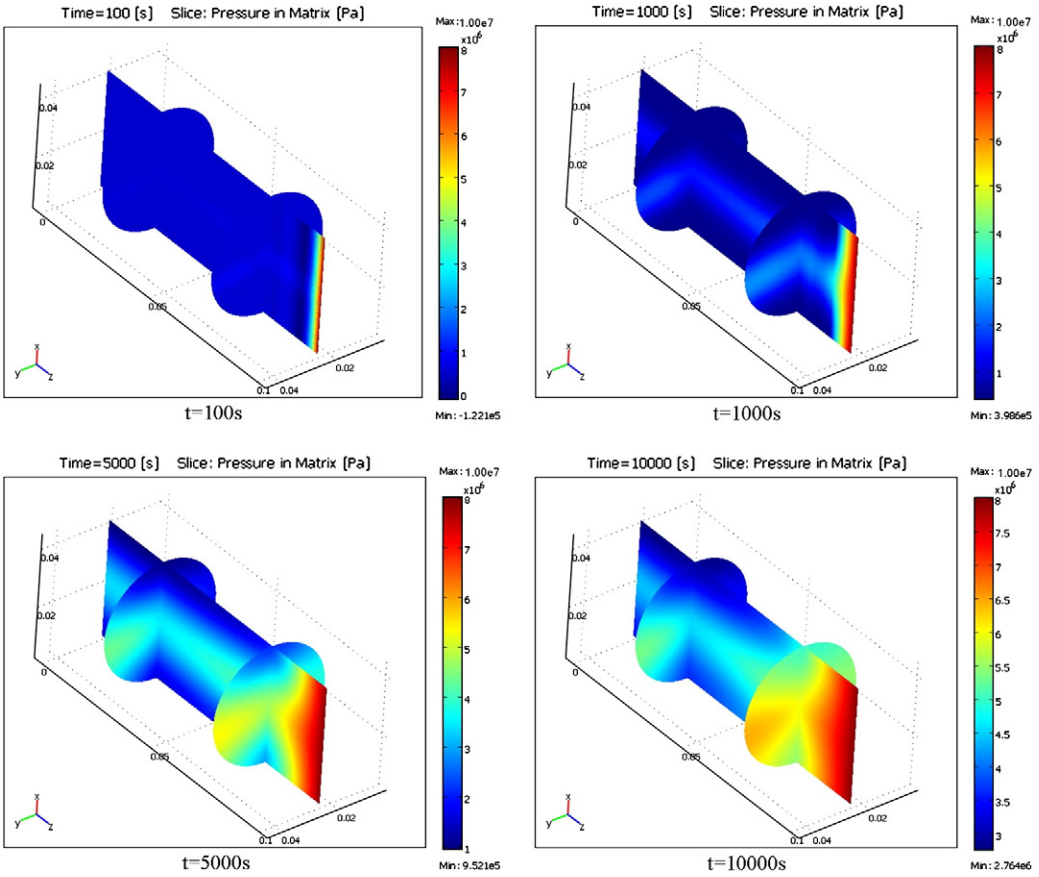

Fig. 13. Characteristics of pressure distribution in the matrix.

evolution of the permeability ratio can be taken as a characteristic of the fracture as it opens and closes. At the beginning of gas injection, the fracture opens due to the dominant influence of the effective stress response — absent swelling. And then as the gas diffuses into the coal matrix and adsorbs to the coal matrix, swelling results in closure of the pores. This swelling results in changes in effective stresses, also — it is the presence of a distribution of porosity and the presence of rock bridges in the fracture that causes changes in effective stresses due to the swelling (Izadi et al., 2010). This behavior is an essential component in driving swelling-induced reduction in permeability.

The comparison between the modeled ensemble permeability and the experimental one is shown in Fig. 10 while the modeled temporal evolution of the ensemble permeability is shown in Fig. 10. When CO_2 is injected into the coal sample the effect of coal swelling induced by gas adsorption has an important impact on permeability — the initial permeability is reduced by about an order of magnitude. The swelling strain makes the micro-fractures and cleats close and the reduction in coal permeability is complete in about the first 20 h of the experiment. Apparent in Fig. 11 is the timing of this permeability change as the invasion of CO_2 from the upstream causes the earliest change in permeability at the upstream sections — ultimately propagating downstream in the sample.

4.2. Characteristics of gas flow

Figs. 12 and 13 show the gas pressure distributions within the fracture and the matrix systems in the coal sample, respectively. The distribution of gas pressure within the sample is controlled by the evolution of permeability — which in turn is a dynamic process. Apparent from Fig. 12 is that when the gas is injected into the coal sample it first fills the high permeability conduits and diffuses from these areas into the surrounding matrix. For the matrix system, although the initial porosity and permeability are homogeneous, the pressure distribution is heterogeneous — it is conditioned by the gas supply from the heterogeneous fracture system. The mechanism of gas transport within the coal matrix is diffusion which is very slow in comparison to transport within the fracture. Therefore, the gas pressure within the matrix system is lower than that in the fracture system from which it is supplied. Figs. 14 and 15 show the pressure distribution along the x-axis in the center of the cylinder. It is clear that the gas flow in the fracture is much faster than in other areas. With progress of the injection the lateral pressure gradients driving flow from the central fracture slowly diminish. The peak injection pressure at mid-length reaches above 5 MPa (the mean of injection and outlet pressures) indicating the role of heterogeneity in the

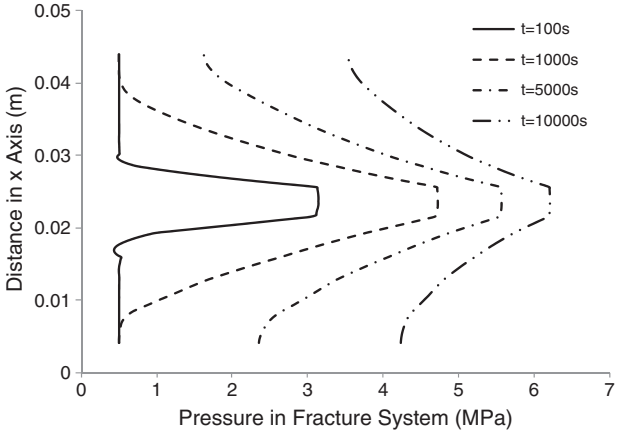

Fig. 14. Pressure distribution in the fracture system along the x-axis in the center of the sample.

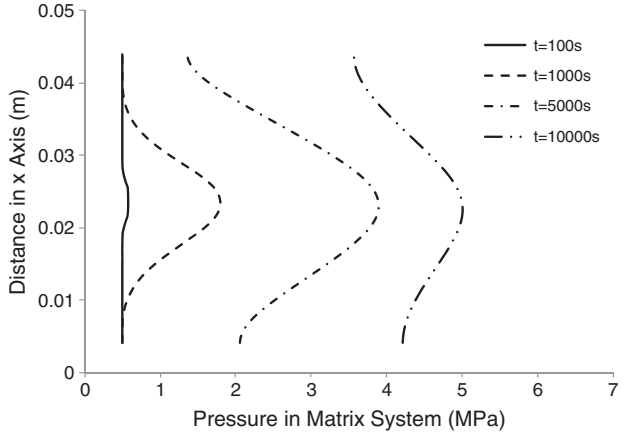

Fig. 15. Pressure distribution in the matrix system along the x-axis in the center of the sample.

steady flow field. With progress of the injection the matrix pressures slowly rise in response to the supply from the controlling main fracture and via micro-fractures. The gas pressure evolution at the center of the coal sample is plotted in Fig. 16. The solid line defines the evolution of pressure within the fracture and dashed line the pressure in the matrix — matrix pressures always lag fracture ones. The ultimate response is the equilibrium between the matrix pressure and the fracture pressure.

5. Conclusions

A dual porosity–dual permeability model has been developed to characterize contributions of various dynamic processes to the CO_2 injection induced evolution of coal permeability. Based on the model results, the following conclusions can be drawn:

- CO2 injection triggers a series of interactive processes, such as matrix swelling, fracture dilation and compaction, and coal stressing and de-stressing. These dynamic processes are heterogeneous. They are controlled primarily by both the initial coal internal structures, such as the distribution of coal fracture, as demonstrated in this study, and the lithotypes present as demonstrated by previous studies.
- The heterogeneous nature of swelling processes determines the obvious discrepancy between the ideal behavior and the practical behavior. When the coal sample is mechanically unconstrained and idealized as a homogeneous system, the ultimate permeability is always greater than the initial one. However, significant reductions are observed as demonstrated in previous studies. For the first time, this study has provided the numerical evidence that the heterogeneity has generated swelling-induced reductions in permeability even when the fractured sample is mechanically unconstrained.

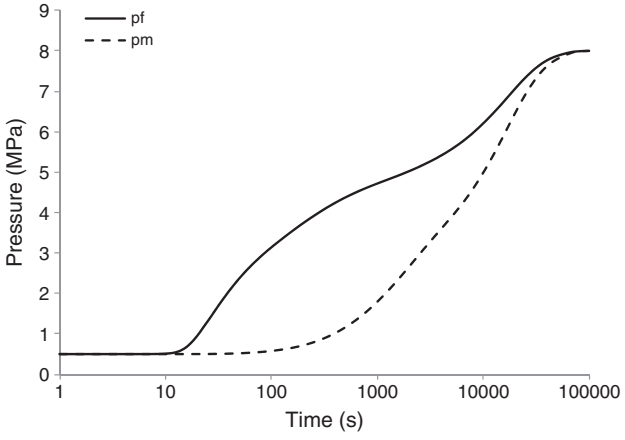

Fig. 16. Pressure evolution of coal sample.

Acknowledgments

This work was supported by the Fundamental Research Funds for the Central Universities (2011QNA17), the Chinese National Natural Science Foundation (50904065), and the State Key Laboratory for Geomechanics and Deep Underground Engineering in China. These sources of support are gratefully acknowledged.

References

Aifantis, E.C., 1977. Introducing a multi-porous medium. Developments in Mechanics 37, 265–296.
Bai, M., Elsworth, D., Roegiers, J.-C., 1993. Multi-porosity/multi-permeability approach to the simulation of naturally fractured reservoirs. Water Resources 29, 1621–1633.
Bai, M., Roegiers, J.-C., Elsworth, D., 1995. Poromechanical response of fractured-porous rock masses. Journal of Petroleum Science and Engineering 13, 155–168.
Bai, M., Elsworth, D., Inyang, H.I., Roegiers, J.-C., 1997. A semi-analytical solution for contaminant migration with linear sorption in strongly heterogeneous media. Journal of Environmental Engineering ASCE 123, 1116–1125.
Barrenblatt, G.I., Zheltov, I.P., Kochina, N., 1960. Basic concepts in the theory of seepage of homogeneous liquids in fissured rocks. Prikl. Mat. Mekh 24 (5), 852–864.
Biot, M.A., 1941. General theory of three-dimensional consolidation. Journal of Applied Physics 12, 155–164.
Busch, A., Gensterblum, Y., Krooss, B.M., Littke, R., 2004. Methane and carbon dioxide adsorption–diffusion experiments on coal: upscaling and modeling. International Journal of Coal Geology 60, 151–168.
Chilingar, G.V., 1964. Relationship between porosity, permeability, and grain size distribution of sands and sandstones. Dev. Sedimentol. 1, 71–74.
Chang, M., Deka, J.R., Tszeng, T.Z., Cheng, P.R., 2008. Online monitoring of pore distribution in microporous membrane. Desalination 234, 66–73.
Charrièrea, D., Pokryszk, Z., Behra, P., 2010. Effect of pressure and temperature on diffusion of CO_2 and CH_4 into coal from the Lorraine basin (France). International Journal of Coal Geology 81 (4), 373–380.
Cui, X., Bustin, R.M., 2005. Volumetric strain associated with methane desorption and its impact on coalbed gas production from deep coal seams. AAPG Bulletin 89, 1181–1202.
Day, S., Fry, R., Sakurovs, R., 2008. Swelling of Australian coals in supercritical CO2. International Journal of Coal Geology 74 (1), 41–52.
Detournay, E., Cheng, A.H.D., 1993. Fundamentals of poroelasticity. In: Fairhurst, C. (Ed.), Comprehensive rock engineering, vol. 2, pp. 113–171.
Douglas Jr., J., Hensley, J.L., Arbogast, T., 1991. A dual-porosity model for water flooding in naturally fractured reservoirs. Computer Methods in Applied Mechanics and Engineering 87, 157–174.
Durucan, S., Shi, J.-Q., 2008. Improving the CO2 well injectivity and enhanced coalbed methane production performance in coal seams. International Journal of Coal Geology 77, 214–221.
Elsworth, D., Bai, M., 1992. Flow-deformation response of dual-porosity mediaÕ. Journal of Geotechnical Engineering ASCE 118, 107–124.
Gale, J., Freund, P., 2001. Coal-bed methane enhancement with CO2 sequestration worldwide potential. Environmental Geosciences 8 (3), 210–217.
Gray, I., 1987. Reservoir engineering in coal seams: part 1 — the physical process of gas storage and movement in coal seams (paper SPE 12514) SPE Reservoir Engineering, pp. 28–34 (February).
Harpalani, S., Schraufnagel, A., 1990. Measurement of parameters impacting methane recovery from coal seams. International Journal of Mining and Geological Engineering 8, 369–384.
Izadi, G., Wang, S., Elsworth, D., Liu, J., Wu, Y., Pone, D., 2010. Permeability evolution of gas-infiltrated coal idealized as a cracked solid. International Journal of Coal Geology 85 (2), 202–211.
Karacan, C.O., 2003. Heterogeneous sorption and swelling in a confined and stressed coal during CO2 injection. Energy and Fuels 17, 1595–1608.
Karacan, C.O., 2007. Swelling-induced volumetric strains internal to a stressed coal associated with CO2 sorption. International Journal of Coal Geology 72, 209–220.
Karacan, C.O., Mitchell, G.D., 2003. Behaviour and effect of different coal microlithotypes during gas transport for carbon dioxide sequestration into coal seams. International Journal of Coal Geology 53, 201–217.
Liu, J., Elsworth, D., 1999. Evaluation of pore water pressure fluctuation around an advancing longwall panel. Advances in Water Resources 22 (6), 633–644.
Liu, J., Elsworth, D., Brady, B.H., 1999. Linking stress-dependent effective porosity and hydraulic conductivity fields to RMR. International Journal of Rock Mechanics and Mining Science 36, 581–596.
Liu, J., Chen, Z., Elsworth, D., Miao, X., Mao, X., 2010a. Linking gas-sorption induced changes in coal permeability to directional strains through a modulus reduction ratio. International Journal of Coal Geology 83 (1), 21–30.

Liu, J., Chen, Z., Elsworth, D., Miao, X., Mao, X., 2010b. Evaluation of stress-controlled coal swelling processes. International Journal of Coal Geology 83 (3), 446–455.
Mazumder, S., Wolf, K.-H., 2007. Differential swelling and permeability change of coal in response to CO2 injection for ECBM. International Journal of Coal Geology 74, 123–138.
Ouyang, Z., Elsworth, D., 1993. Evaluation of groundwater flow into mined panels. International Journal of Rock Mechanics and Mining Science and Geomechanics 30, 71–80.
Palmer, I., 2009. Permeability changes in coal: analytical modelling. International Journal of Coal Geology 77, 119–126.
Palmer, I., Mansoori, J., 1998. How permeability depends on stress and pore pressure in coalbeds: a new model. Paper SPE 52607 SPE Reservoir Evaluation & Engineering, pp. 539–544 (December).
Pekot, L.J., Reeves, S.R., 2003. Modeling the effects of matrix shrinkage and differential swelling on coalbed methane recovery and carbon sequestration. Paper 0328, proc. 2003 International Coalbed Methane Symposium. University of Alabama, Tuscaloosa, Alabama, p. 1 (May).
Pili, E., Perrier, F., et al., 2004. Dual porosity mechanism for transient groundwater and gas anomalies induced by external forcing. Earth and Planetary Science Letters 227, 473–480.
Pone, J.D.N., Hile, M., Halleck, P.M., Mathews, J.P., 2008. Three-dimensional carbon dioxide-induced strain distribution within a confined bituminous coal. International Journal of Coal Geology 77, 103–108.
Prusty, B.K., 2007. Sorption of methane and CO_2 for enhanced coalbed methane recovery and carbon dioxide sequestration. Journal of Natural Gas Chemistry 17, 29–38.
Robertson, E.P., Christiansen, R.L., 2005. Measurement of sorption-induced strain. International Coalbed Methane Symposium. University of Alabama, Tuscaloosa (Paper 0532).
Robertson, E.P., Christiansen, R.L., 2007. Modeling laboratory permeability in coal using sorption-induced-strain data. SPE Reservoir Evaluation and Engineering 10 (3), 260–269.
Seidle, J.P., Huitt, L.G., 1995. Experimental measurement of coal matrix shrinkage due to gas desorption and implications for cleat permeability increases. Paper SPE 30010, presented at the 1995 International Meeting on Petroleum Engineering, Beijing, China (14–17 November).
Shi, J., Durucan, S., 2005. A model for changes in coalbed permeability during primary and enhanced methane recovery. SPE Reservoir Evaluation and Engineering 8, 291–299.
Siemons, N., Busch, A., 2007. Measurement and interpretation of supercritical CO2 sorption on various coals. International Journal of Coal Geology 69 (4), 229–242.
Siriwardane, H., Haljasmaa, I., McLendon, R., et al., 2009. Influence of carbon dioxide on coal permeability determined by pressure transient methods. International Journal of Coal Geology 77, 109–118.
Wang, G.X., Massarotto, P., Rudolph, V., 2009. An improved permeability model of coal for coalbed methane recovery and CO2 geosequestration. International Journal of Coal Geology 77 (2009), 127–136.
Warren, J.E., Root, P.J., 1963. Behavior of naturally fractured reservoirs. Society of Petroleum Engineers Journal 228, 245–255.
Wu, Y., Liu, J., Chen, Z., et al., 2009. Dual poroelastic response of coal seam to CO2 injection. 43rd U.S. Rock Mechanics Symposium and 4th U.S.–Canada Rock Mechanics Symposium, Asheville, NC (June 28th – July 1, 2009).
Wu, Y., Liu, J., et al., 2010a. Dual poroelastic response of a coal seam to CO_2 injection. International Journal of Greenhouse Gas Control 4 (4), 668–678.
Wu, Y., Liu, J., et al., 2010b. Development of anisotropic permeability during coalbed methane production. Journal of Natural Gas Science and Engineering 2 (2010), 197–210.
Zhang, H.B., Liu, J., Elsworth, D., 2008. How sorption-induced matrix deformation affects gas flow in coal seams: a new FE model. International Journal of Rock Mechanics & Mining Sciences 45, 1226–1236.
Zhao, Y.S., Hu, Y.Q., Zhao, B., Yang, D., 2004. Nonlinear coupled mathematical model for solid deformation and gas seepage in fractured media. Transport Porous Media 55, 119–136.
Zimmerman, R.W., Somerton, W.H., King, M.S., 1986. Compressibility of porous rocks. Journal of Geophysical Research 91, 12,765–12,777.